Available online at www.sciencedirect.com
SCIENCE DIRECT
Thin Solid Films 503 (2006) 167 – 176
thin solid films
www.elsevier.com/locate/tsf

Buckle morphology of compressed inorganic thin layers on a polymer substrate

A.A. Abdallah [a,*], D. Kozodaev [b,d], P.C.P. Bouten [c], J.M.J. den Toonder [c], U.S. Schubert [b], G. de With [a]

[a] Laboratory of Materials and Interface Chemistry, Eindhoven University of Technology, Den Dolech 2, 5600 MB Eindhoven, The Netherlands
[b] Laboratory of Macromolecular Chemistry and Nano Science, Eindhoven University of Technology, Den Dolech 2, 5600 MB Eindhoven, The Netherlands
[c] Philips Research Laboratories, Prof. Holstlaan 4, 5656 AA Eindhoven, The Netherlands
[d] NT-MTD Co./NTI-Europe, Arnhemseweg 34 d, 7331 BL Apeldoorn, The Netherlands

Received 4 May 2005; received in revised form 14 October 2005; accepted 29 November 2005
Available online 7 February 2006

Abstract

The structural integrity of thin-film multi-layer structures that are used, e.g. in displays are of paramount importance. Layer buckling and delamination is a common interfacial failure phenomenon in these structures. In this paper plasma enhanced chemical vapor deposition has been used to grow a silicon nitride layer (Si_3N_4), 400 nm thick, on a high temperature aromatic polyester substrate spin coated with a silica–acrylate hybrid coating. Two-loading mechanisms are discussed: biaxial-compressive residual stress and uniaxial-compressive external stress. The influence of loading mechanism and level of adhesion on buckle morphology has been investigated. Telephone-cord and straight buckling are observed when the layer was under biaxial-compressive residual stress while circular buckling is observed when the layer was under additional uniaxial-compressive external stress. Oxygen plasma treatment is found to enhance buckling of the Si_3N_4 layer from the polymer substrate. The buckle width and heights are found to increase with the uniaxial-compressive external strain.

Keywords: Multi-layers; Elastic properties; Adhesion; Delamination

1. Introduction

Flexible displays are multi-layered structures consisting of a polymer-based substrate sandwiched between a number of functional layers that act as a gas barrier layer, e.g. an inorganic thin layer, and a transparent conducting oxide layer. For flexible displays the mechanical integrity of these multi-layer structures and their reliability is important. Each layer has its own material properties that contribute to the mechanical response of the complete structure. Generally, the inorganic layers have a higher elastic modulus and a lower thermal expansion coefficient as compared with the polymer substrate. As a result of this dissimilarity and the high deposition temperature, residual stresses are present in the layered structure. High compressive stresses in the thin layer in combination with insufficient adhesion at the interface can cause the layer to buckle and to delaminate from the substrate. These buckling phenomena are undesirable from a functional and reliability point of view and therefore should be avoided.

In the framework of buckling theory for a beam clamped on both edges, numerous buckle morphologies have been studied for various thin layer structures on substrates, often neglecting the effect of the substrate's deformation [1–7]. Recently, Cotterell and Chen [8] and Yu and Hutchinson [9] have shown that for a stiff layer buckled from a compliant substrate under compressive strain, the elastic energy release rate from the substrate can be more than an order of magnitude greater than the value obtained neglecting the substrate's deformation. The more compliant the substrate, the easier for the layer to buckle and the higher the energy release rates. Buckling of metallic thin layer from a polymer substrate under tensile stresses has also been reported [10].

The process of buckle formation and subsequent buckle growth can be explained as a release of elastic strain energy

* Corresponding author.
E-mail address: a.abdallah@tue.nl (A.A. Abdallah).

0040-6090/$ - see front matter © 2005 Elsevier B.V. All rights reserved.
doi:10.1016/j.tsf.2005.11.106

stored in the layer. This reduction results from relaxation of stress components in the layer (σ_{xx} and σ_{yy}), therefore, the stress components in the layer are considered parameter in layer buckling and delamination. In this paper attention is paid to the influence of loading mechanism and level of adhesion on buckle morphology. Different types of buckle profiles are presented and the buckle evolution mechanism associated with the applied stress is discussed.

2. Experimental details

2.1. Materials

The material system consists of a polymer substrate (Arylite™) spin coated on both sides with a silica–acrylate hybrid coating (hereafter referred to as "Hard Coat"). These layers improve the mechanical properties of the layered structure and act as a solvent barrier.

Plasma enhanced chemical vapor deposition has been used to grow silicon nitride layers (Si_3N_4) on the Hard Coat. This layer acts as a gas barrier. To achieve different levels of adhesion, the Si_3N_4 layers were deposited with and without oxygen plasma treatment of the Hard Coat surface prior to layer deposition.

A summary of the material parameters and thickness is given in Table 1. The elastic modulus of the Hard Coat was derived from the moduli of a 12 μm thick PET substrate spin coated with and without a 1.03 μm thick Hard Coat [11]. The elastic modulus of the substrate material has been measured using a homemade nanoindentation device described in Ref. [12].

Two-loading mechanisms will be introduced: a layer under biaxial-compressive residual stress and a layer under uniaxial-compressive external stress.

2.2. Layer under biaxial-compressive residual stress

The residual stresses induced in the Si_3N_4 layers during deposition σ_f, have been estimated using the analysis of Röll [13]; which accounts for the elastic modulus of the layer:

$$\sigma_f = \frac{E_s}{6(1-\nu_s)}\frac{h_s^2}{h_f}\left[\frac{1}{R_2}-\frac{1}{R_1}\right]\left[1+\frac{h_f}{h_s}\left(4\frac{E_f}{E_s}-1\right)\right] \tag{1}$$

where E_s, ν_s and h_s are the elastic modulus, Poisson's ratio and thickness of the substrate, respectively, E_s, h_f are the elastic modulus and the thickness of the layer, respectively. R_1 and R_2 are the radius of curvature before and after deposition of the layer, respectively. Since the bare substrate was flat, we used, $R_1 \cong 0$. The substrate radius of curvature R_2 has been measured by placing the specimen under an optical microscope and making an image of the substrate curvature. From the image the radius of curvature was determined by image processing analysis. Using the data reported in Table 1, the residual stresses in the thin layer σ_f were calculated from Eq. (1) and is given in Table 2.

For a layer clamped on both edges, buckling may occur when the compressive stress exceeds the critical buckling stress, which is given by [1]:

$$\sigma_c = \frac{\pi^2 E_f}{12\left(1-\nu_f^2\right)}\left[\frac{h_f}{b}\right]^2 \tag{2}$$

where E_f, ν_f and h_f are the elastic modulus, Poisson's ratio and thickness of the layer, respectively, and b is the half width of the buckle (Fig. 1).

Therefore, in thin-film mechanics a high residual stress in the thin layer in combination with insufficient adhesion at the interface can be sufficient to initiate layer buckling without externally applied stress [14,15].

2.3. Layer under uniaxial-compressive external stress

A mechanical bending device, shown in Fig. 2, has been used to apply deformation with constant curvature over a length of about 2.5 cm to the layered structures. As a result, the substrate is loaded in tension at the outer surface and in compression at the inner surface. Changing the distance

Table 1
Material constants

Material	Elastic modulus, GPa	Poisson's ratio	Thickness, μm
Arylite™	3.0	0.38[a]	200
Hard Coat	6.5	0.3[a]	3
Si_3N_4 layer	150*	0.3[a]	0.2, 0.3 and 0.4

[a] Estimated values [11].

Table 2
An overview of the results

Layer thickness h_f, μm	Substrate curvature R_2, mm	Residual stress in the layer σ_f, GPa	Oxygen plasma treatment	Buckle morphology
0.2	188±6	1.03±0.03	+	Intact
0.3	98±3	1.42±0.04	+	Telephone-cord, straight
0.4	123±40	0.92±0.23	+	Telephone-cord
0.2	188±6	1.03±0.03	–	Intact
0.3	98±3	1.42±0.04	–	Intact
0.4	123±40	0.92±0.23	–	Intact

Estimation of the residual stresses induced in the Si_3N_4 layer during deposition using Röll analysis and measured substrate curvature. Layers were deposited with and without oxygen plasma treatment. Buckle morphology results from layer processing.

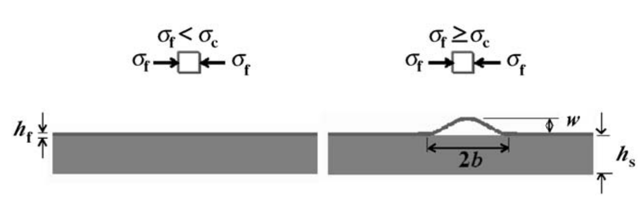

Fig. 1. Illustration of buckling of compressed layer: (left) the layer is attached to the substrate for residual stress below the critical buckling stress; (right) layer buckling can occur only when the residual stress becomes equal or larger than the critical buckling stress. The thickness of the layer and the substrate is given in Table 1.

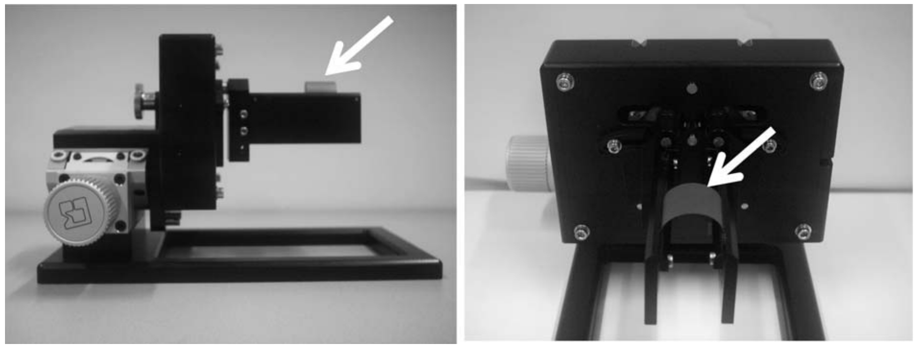

Fig. 2. The mechanical bending device used to deform the layered structure, indicated by an arrow that is mounted between two bending plates.

between the bending plates will change the strain applied to the layered structure.

For thin brittle layers on polymer substrates, the critical strain is more representative than stress for characterizing failure. This is due to the time-dependent behavior of the polymer substrate, e.g., when a sample shows viscoelastic behavior, the stress will be relaxed while the applied strain is constant.

Assuming that the neutral line is located at the mid-plane of the layered structure, the strain applied ε *can* be calculated from Ref. [16]:

$$\varepsilon = \frac{(h_s + h_f)}{2R} \tag{3}$$

where h_s and h_f are the thickness of the substrate and the layer, respectively, and R is the bending radius. At a constant bending radius R, Eq. (3) gives a constant strain along the sample length.

Again, for a layer clamped on both edges, buckling occurs when the uniaxial–applied external stress exceeds the critical buckling stress. Using the relation between stress and strain for a plate with Young's modulus E and Poisson's ratio v ($\sigma = E\varepsilon/(1-v^2)$) and Eq. (2), the corresponding critical buckling strain can be calculated by:

$$\varepsilon_c = \frac{\pi^2}{12}\left[\frac{h_f}{b}\right]^2 \tag{4}$$

Layer buckling occurs to release the elastic energy stored in the layer during deposition and/or by applying an external stress. The elastic energy G_o stored in a thin layer per unit width is defined by [1]:

$$G_o = \frac{1}{2}\frac{E_f}{\left(1-v_f^2\right)}\varepsilon^2 h_f \tag{5}$$

The residual strain in the buckled layer is approximately equal to the critical buckling strain ($\varepsilon_o \cong \varepsilon_c$) and therefore,

$$G_c = \frac{1}{2}\frac{E_f}{\left(1-v_f^2\right)}\varepsilon_c^2 h_f \tag{6}$$

The steady-state energy release rate of the advancing buckle G_{ss} is an important parameter to describe layer buckling and delamination. From a fracture mechanics point of view, delaminatinon is expected to occur when G_{ss} exceeds the interfacial toughness Γ_i [1]:

$$G_{ss} = G_o\left[1-\frac{\varepsilon_c}{\varepsilon}\right]^2 \geq \Gamma_i \tag{7}$$

Dundurs [17] has defined two elastic mismatch parameters. For our application the more important is the first parameter α defined for plane-strain problems as:

$$\alpha = \frac{E_f' - E_s'}{E_f' + E_s'} \tag{8}$$

where, E_s' and E_f' are the plane-strain Young's moduli for the substrate and the layer, respectively. The second Dundurs'

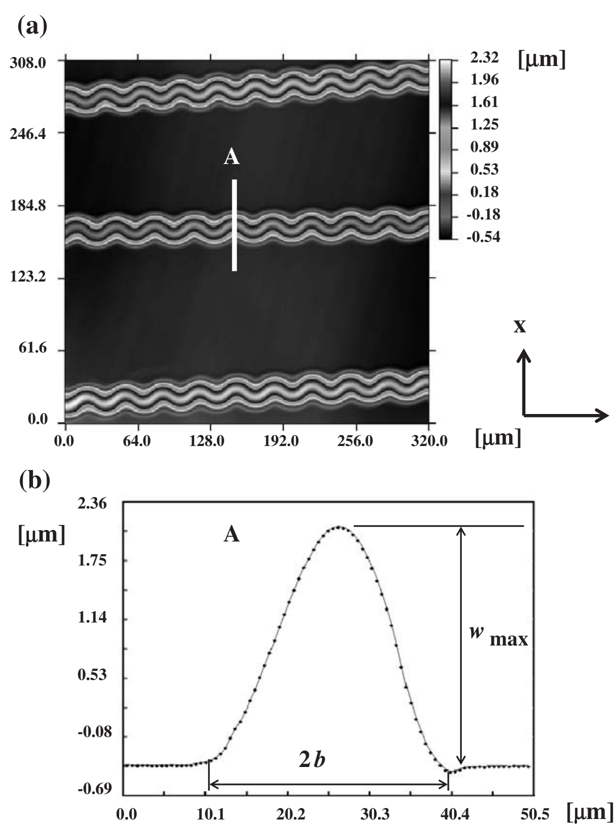

Fig. 3. Confocal microscope images obtained for telephone-cord buckles without layer cracking formed due to biaxial–residual compressive stress in a 400 nm thick Si_3N_4 layer with oxygen plasma treatment: (a) 2-D image and (b) buckle profile measured along the center of the buckle, line A.

parameter β is well approximated for the present configuration by $\beta = \alpha/4$. Note that, for an elastic layer on a rigid substrate $\alpha \to -1$, for a homogenous elastic system $\alpha \to 0$, and for a stiff layer on a compliant substrate $\alpha \to +1$. In our case, the Si_3N_4 layer on the Hard Coat results in $\alpha = 0.917$. Therefore, the effect of the substrate compliance on layer buckling should be considered.

For a stiff layer on a compliant substrate, the elastic energy release over a certain width of the layer still attached to the substrate along the edge of the delamination contributes to the buckling and delamination process. This width scales with a characteristic length [9]: $l = 2h_f/[1-\alpha]$.

More recently, Bouten and van Gils [18] have shown significant lowering of the critical strain for a stiff layer on a compliant substrate. The energy balance for buckling can be written as [18]:

$$2bG_{ss} = 2(b + l)(G_o - G_c) \quad (9)$$

In this approximation the elastic energy released from the substrate is neglected. The right hand term describes the energy release in the thin layer upon buckling as a function of the effective buckle length ($b + l$), which depends on the layer thickness and the elastic mismatch. As a consequence significantly more elastic energy is available for buckling formation. The left hand term represents the energy required for delamination. The energy release in the thin layer upon buckling has to exceed the energy required to form a new free surface.

As a result, the buckle onset strain defined at a given quality of adhesion for a compliant substrate is lower than the one predicted by the model for a rigid substrate [1]. Apart from that, the critical buckling strain ε_c will be reduced for a stiff layer on a compliant substrate due to the rotation and the displacement at the buckle edges.

2.4. Atomic force microscopy (AFM) and confocal microscopy measurements

The buckle morphology and profiles were measured by atomic force microscopy AFM (Solver-LS, NT-MDT) and confocal optical microscopy (NanoFocus).

The AFM system is equipped with $120 \times 120 \times 12$ μm piezo-scanner, moving positioning stage (Ø 250 mm) and optical system with 1.5 μm resolution. The AFM images were obtained in semi-contact and local elasticity modes with silicon tips (NSG01S produced by NT-MDT).

The confocal optical microscope (NanoFocusX® μSurf®) is equipped with a piezo-drive. The measurement field of the microscope is depicted to 512×512 pixels. Using a measurement field of 140×132 μm; a lateral resolution of 0.2 μm is

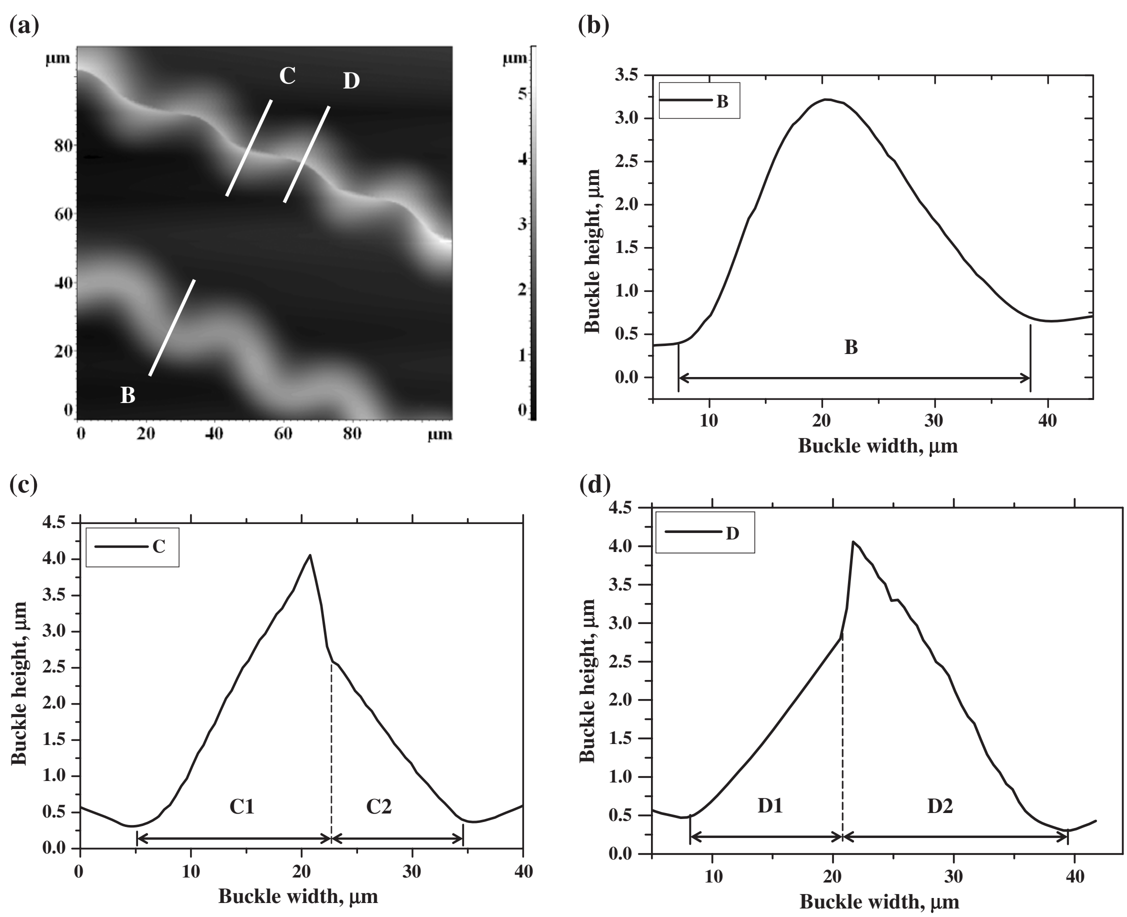

Fig. 4. (a) 2-D image of telephone-cord buckles of 400 nm thick Si_3N_4 layer on a compliant substrate, (b) buckle profiles for the telephone-cord with and without the layer cracking, (c) and (d) buckle profile for the telephone-cord with the layer cracking taken from the same direction C, line C and line D, respectively.

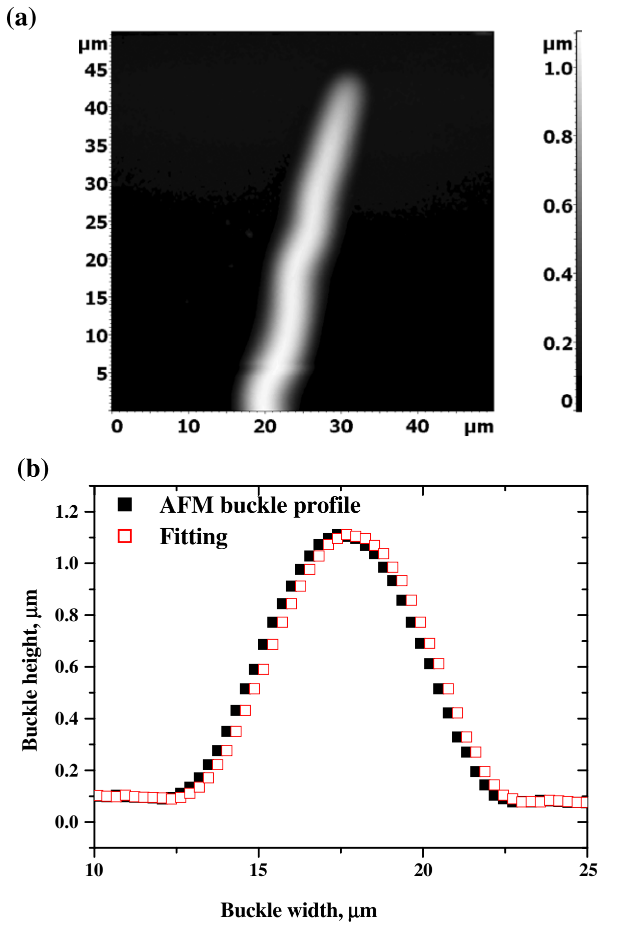

Fig. 5. (a) 2-D image of the straight buckle due to biaxial-compressive residual stress on Si_3N_4 layer after oxygen plasma treatment, (b) AFM buckle profile fitted with Eq. (10). The buckle width $2b=9.7$ µm, the buckle height $w=0.88$ µm.

obtained while by means of the piezo-drive, a vertical resolution of 0.1 µm is obtained.

3. Results and discussions

In this section, we will discuss the results of layer buckling and delamination. An overview of the results is given in Table 2. Our focus will be mainly on buckle morphology with and without layer cracking; different types of buckle profiles are presented. Furthermore, the buckle evolution mechanism associated with the applied stress is discussed.

From the AFM and the confocal microscope images no delamination of the Hard Coat from the polymer substrate were observed. By measuring the thickness of the delaminated layer we found that only the Si_3N_4 layer is delaminated and buckled from the Hard Coat.

3.1. Buckling and delamination of thin layer under biaxial-compressive residual stress

There are many parameters controlling buckling and delamination due to residual stress [19,20]; we will consider only the magnitude of residual stress, layer thickness and the properties of the interface.

3.1.1. Telephone-cord patterns with and without layer cracking

Sinusoidal buckling, known as a telephone-cord and shown in Fig. 3, resulting from the biaxial–residual stress was observed after deposition of a 400 nm thick Si_3N_4 layer, using a preceding oxygen plasma treatment. For this particular layer thickness the residual stress is estimated to be 0.92 GPa. From the buckle profiles (Fig. 3b) the average of the buckle width ($2b=31\pm1$ µm) and height ($w=2.5\pm0.1$ µm), are determined perpendicular to the buckle axis (line A).

Fig. 3a can be used to explain the formation of the telephone-cord buckles. Suppose that buckling occurs in the x-direction. In this case the uniaxial stress is relaxed in this direction and $\sigma_{xx}\cong\sigma_c$. After buckling, a compressive stress is still present in the y-direction; $\sigma_{yy}\cong-(1-\nu)\sigma_f$, which may cause a secondary buckling that is responsible for formation of the sinusoidal buckle [21]. Moreover, due to the biaxially compressed layer on one side of the substrate, the sample is curved. As a result, the biaxial-compressive

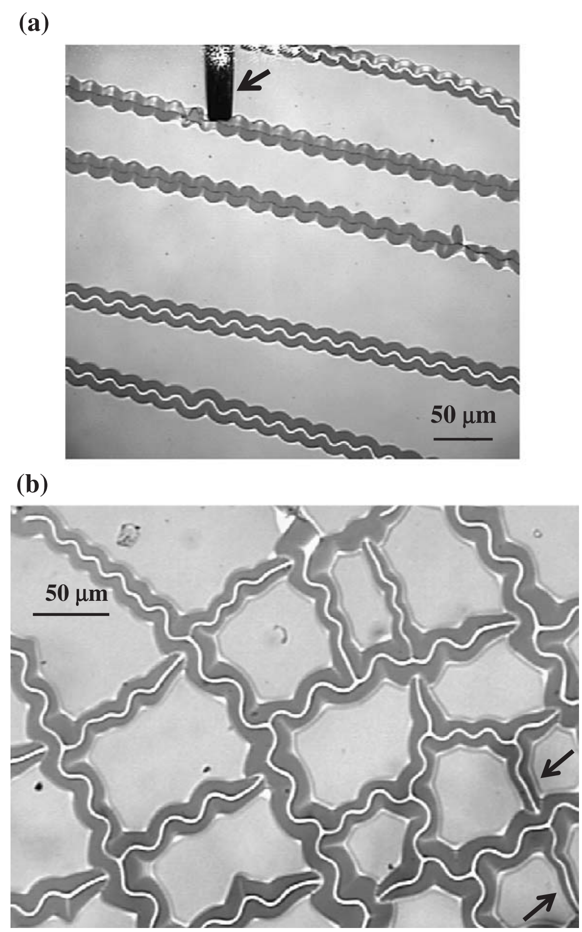

Fig. 6. (a) Optical micrographs of the telephone-cord buckle with and without layer cracking using the AFM system (the cantilever is indicated with the arrow). (b) Telephone-cord buckle split up and formed network. Small straight buckles are also observed (indicated with the arrow).

stress is slightly released in one direction “normal to the curvature axis”.

An oxygen plasma treatment has been found to improve adhesion of coatings for different polymers by producing oxygen groups on the polymer surface [22]. In contrast to that, in this work oxygen plasma treatment is found to enhance buckling of the Si_3N_4 layer. Layers prepared with oxygen plasma treatment (power: 600 W, time: 1 min) showed spontaneous buckling and delamination. Degradation of the superficial layer of the Hard Coat occurred. Mechanism of the effect of oxygen plasma treatment prior to layer deposition on buckling and delamination is subject of forthcoming study. On the other hand, layers prepared without oxygen plasma treatment remained completely attached to the substrate.

For a compliant substrate the total energy release rate is the sum of the energy released from the layer and the energy released from the substrate. The energy release rate can be used to delaminate the layer from the substrate but might also be used to crack the buckled portion of the layer. Therefore, layer cracking provides another mechanism for the total energy stored in the layered structure to be released [16].

Telephone-cord buckles accompanied with layer cracking were also observed for the 400 nm thick Si_3N_4 layer, using an oxygen plasma treatment. Comparing the telephone-cord buckles without layer cracking, indicated in Fig. 4 by line B, and the telephone-cord buckles with layer cracking, indicated in Fig. 4 by line C and line D, reveals the following:

- From the buckle profiles, layer cracking is evident in the buckled portion of the layer as a sharp transition point. As a result, the buckle width is divided to two unequal parts.
- As a consequence of layer cracking an increase in the buckle height is observed from 2.5 μm for the telephone-cord without layer cracking to 4 μm for the telephone-cord with layer cracking. This corresponds with a decrease in the buckle width from 33.7 μm for the telephone-cord without layer cracking to 30 μm for the telephone-cord with layer cracking.
- The cracked telephone-cord buckle is asymmetric about its centerline.

Buckling accompanied with layer cracking will occur when the stress in the buckled portion of the layer exceeds the fracture stress of the layer. The maximum stress in the buckle may be dependent on the distance between buckles. From Fig. 3, the distance between telephone-cord buckles without film cracking is approximately three times the buckle width. On the other hand, for the telephone-cord buckles with film cracking (Fig. 4), the distance between buckles is less than the buckle width.

3.1.2. Straight buckle

Both straight and telephone-cord buckles were observed for the 300 nm Si_3N_4 layer after oxygen plasma treatment. Fig. 5 shows the straight buckle generated due to biaxial-compressive residual stress.

For a straight buckle, the displacement $w(x)$ of the buckled layer from the substrate can be approximated by [23,24]:

$$w(x) = \frac{w_{\max}}{2}\left[1 + \cos\left\{\frac{\pi x}{b}\right\}\right] \tag{10}$$

where $w_{\max}$ and b are the maximum height and the half width of the straight buckle, respectively. Fig. 5b shows that the buckle profile as measured with AFM can be fitted well with Eq. (10).

From the above observations, layer buckling due to the biaxial-compressive residual stress is well established. We have seen that the effect of the level of adhesion at the interface is significant. Poor adhesion results in a spontaneously telephone-cord buckle shape. The occurrence of telephone-cord or straight buckle depends on the ratio of the residual stress to the critical buckling stress. Moon et al. [5] proposed that the residual strain in the layer has to exceed the critical buckling strain by a factor of four for the telephone-cord to exist. In our case considering the telephone-cord buckles shown in Fig. 3, based on the elastic modulus of the layer (Table 1) and the stress determined in Table 2, residual strains of 0.43% is obtained. By assuming the delaminated layer is clamped at its edges, critical buckling strain of 0.05% is derived, thus the

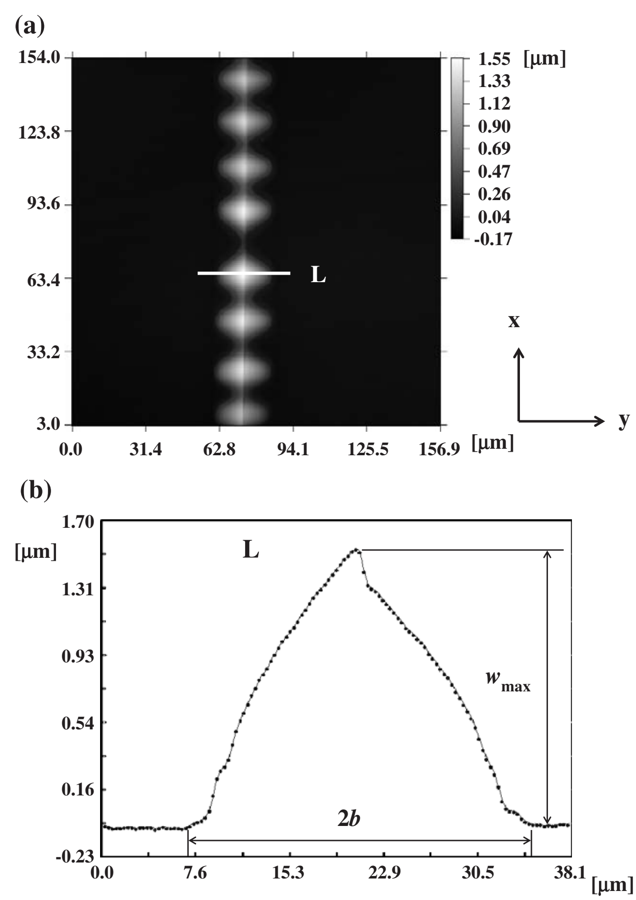

Fig. 7. Confocal microscope images obtained for circular buckle with layer cracking resulting from uniaxial-compressive external stress along the y-axis. The Si_3N_4 layer thickness is 200 nm deposited without oxygen plasma treatment. (a) 2-D image, (b) buckle profile measured along the measured along the center of the buckle, line L.

telephone-cord is found to exist when the residual strain is approximately 9 times the critical buckling strain. The ratio is thus significantly above the ratio proposed by Moon et al. [5]. From the other hand, considering the straight buckle shown in Fig. 5 (residual strain = 0.66%, critical buckling strain = 0.31%) the straight buckle is found to exist when the residual strain is approximately 2 times the critical buckling strain.

For a stiff layer on a compliant substrate the critical buckling strains will be reduced due to the rotation and the displacement at the buckle edges. Therefore, telephone-cord buckles of a stiff layer on a compliant substrate will occur at lower residual strain than in the case of a rigid substrate. Straight buckling is found to occur at low compressive strain level.

The telephone-cord type patterns were observed to split up and form a network, the resulting structures having a characteristic dimension of a few times the buckle width, as can be seen in Fig. 6.

Finally, the 200 nm Si_3N_4 layer prepared with oxygen plasma treatment remained completely attached to the substrate. A reasonable estimation of the adhesion energy for this particular thickness is obtained by assuming that different buckles were generated having different buckle width. By plotting the adhesion energy G_{ss} versus the buckle width, the values of the adhesion energy have been found to a reach a minimum of 0.5 J/m^2 at a buckle width of 31 μm. In comparison with the adhesion energy of the 400 nm Si_3N_4 layer prepared with oxygen plasma treatment that showed spontaneous buckling and delamination (Fig. 3) $G_{ss} \cong 0.4$ J/m^2.

3.2. Buckling and delamination of thin layer under uniaxial-compressive external stress

The Si_3N_4 layers deposited without oxygen plasma treatment remaining attached to the substrate in spite of the presence of the biaxial-compressive residual strain in these layers. Uniaxial-compressive external strain has been applied to these layers using the mechanical bending device shown in Fig. 2. Therefore, the total strain is the sum of the biaxial-compressive residual strain and the uniaxial-compressive applied strain. Due to the uniaxial-compressive applied strain lines of circular, half-circular and semi-circular buckles with layer cracking were observed perpendicular to the compression axis, as shown in Figs. 7–11. Straight buckles are also observed.

Firstly, ex situ experiments have been conducted to study the initiation of the circular buckle. The Si_3N_4 layer thickness is 400 nm deposited without oxygen plasma treatment. A

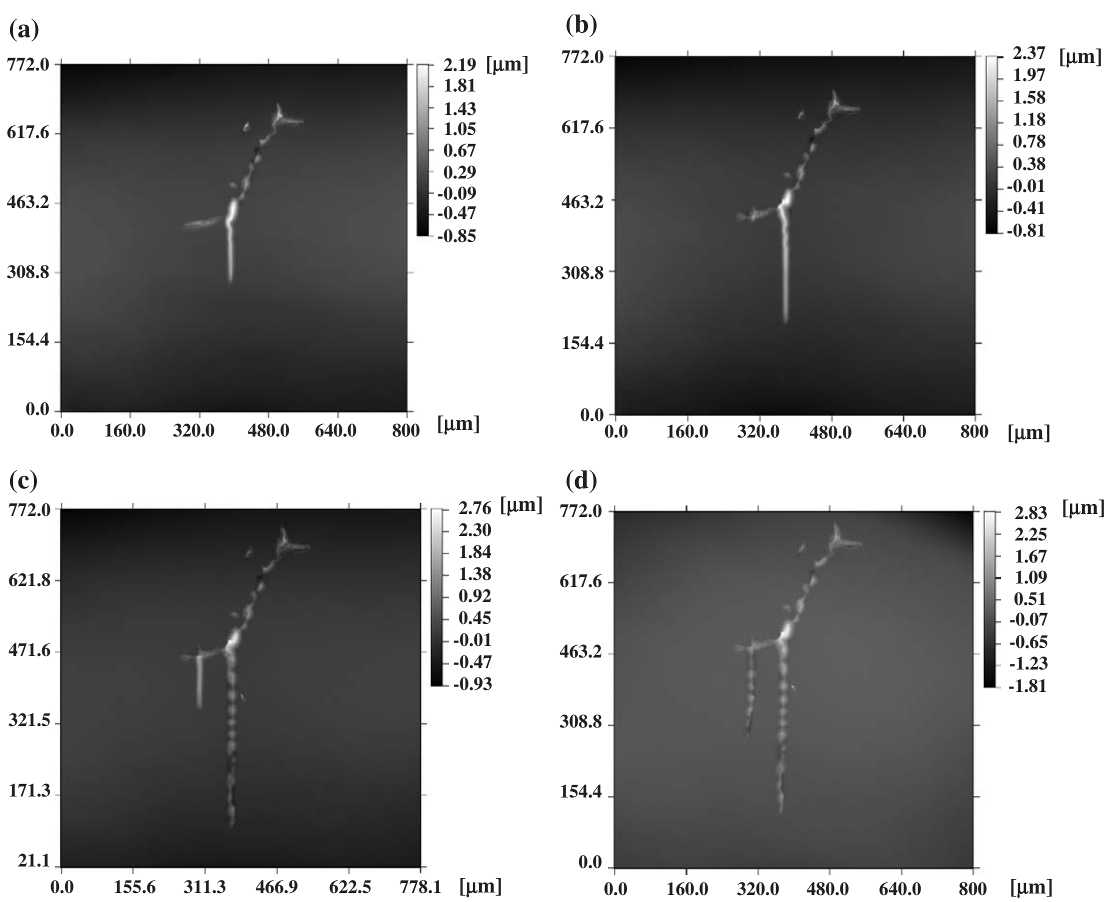

Fig. 8. Confocal microscope images showing the transition from straight buckle to circular buckle by increasing the compressive-strain. Images have been taken after bending, i.e. from a flat sample: (a) ε = 1.35%, (b) ε = 1.46%, (c) ε = 1.62%, (d) ε = 1.85%. The Si_3N_4 layer is 400 nm thick and deposited without oxygen plasma treatment.

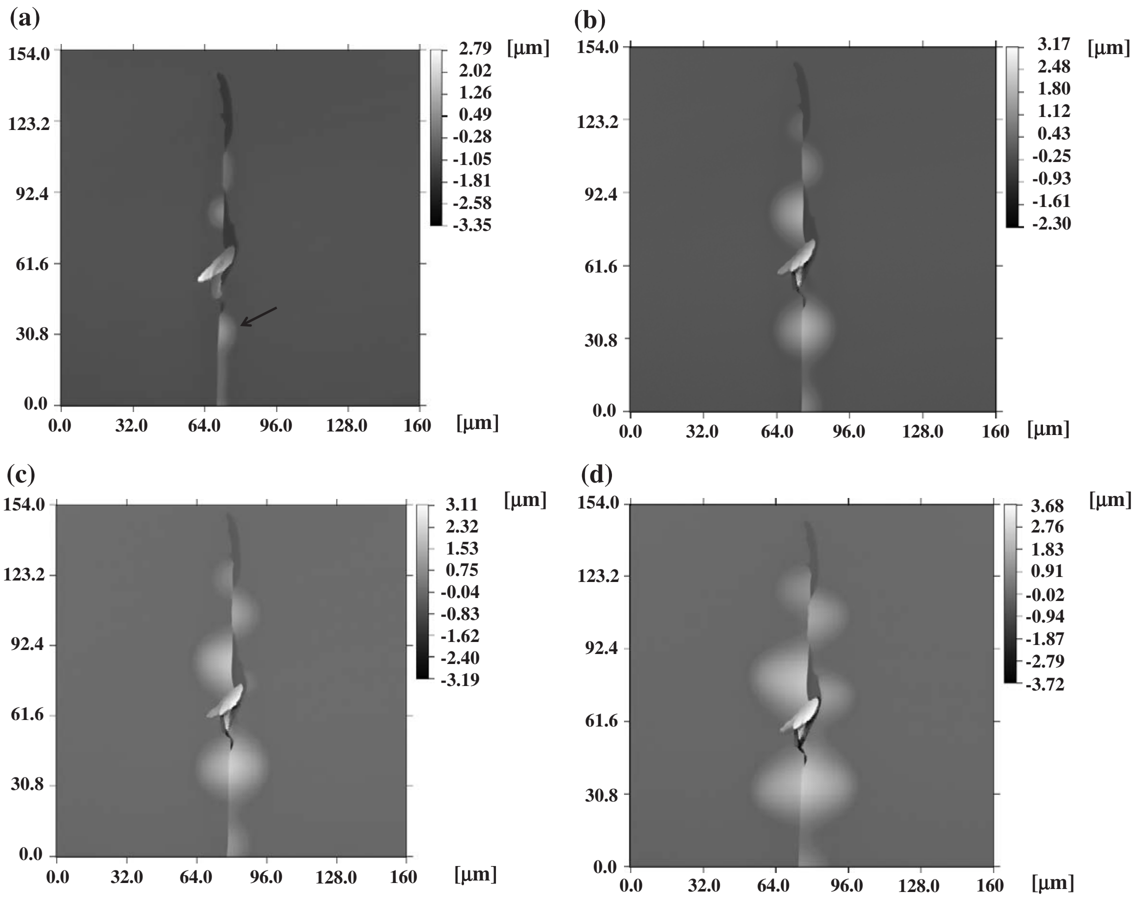

Fig. 9. Confocal microscope images showing the evolution of a half-circular buckle, indicated with an arrow, to circular and semi-circular buckle by increasing the uniaxial-compressive strain. Images have been taken after bending, i.e. from a flat sample: (a) ε = 1.24%, (b) ε = 1.3%, (c) ε = 1.36%, (d) ε = 1.6%. The Si_3N_4 layer is 400 nm thick and deposited without oxygen plasma treatment.

circular buckle is found to be initiated as a straight buckle and then evolve to a circular buckle by increasing the total compressive strain from 1.35% to 1.85% (Fig. 8). Both straight and circular buckles are accompanied with layer cracking on top. New buckles are also observed parallel to each other.

Secondly, experiments have been conducted to study the evolution of the different buckle patterns during propagation. The Si_3N_4 layer thickness is 400 nm deposited without oxygen plasma treatment. From Fig. 9, it is obvious that half-circular buckles may develop to circular or semi-circular buckling. By increasing the applied compressive strain from 1.24% to 1.36%, the half-circular buckle, indicated with an arrow in Fig. 9a, evolves to a circular buckle (Fig. 9c). A transition from circular to semi-circular buckle morphology (Fig. 9d) occurs by further increasing the applied strain up to 1.6%. During this process the buckle height is increased from 1 to 2.8 µm, and the buckle width from 11 to 49 µm. These types of buckles are suggested to be initiated from layer cracking observed perpendicular to the compression axis.

Lastly, in situ observations of the layer buckling during a constant unaxial-compressive stress have been conducted using the optical microscope. Images have been captured with intervals of 5 s (these images are not shown in this paper). From the in situ observation we have seen that buckling starts first to develop in the lateral direction. Next, after the buckle reaches a critical half width, the buckle jumps instantaneously perpendicularly to the compression axis with a nearly constant step to form another periodic series of circular, half-circular or semi-circular patterns. This process is governed by several parameters, for instance, the applied compressive strain, the time needed for the buckle to reach the half critical width and the presence of defects, imperfections or adjacent buckles.

Fig. 10 shows asymmetric semi-circular buckle resulting from applying a compressive strain of 1.52% on the 400 nm thick Si_3N_4 layer. From the buckle profile layer cracking is evident as a sharp transition point. This point can be used to characterize the buckle morphology accompanied with layer cracking, which splits the circular buckle asymmetrically to two alternating parts. In addition, the buckle width E1 approximately equals F2; and buckle width E2 equals F1. The same is valid for the buckle height.

Fig. 11 shows buckling of 300 nm thick Si_3N_4 layer from the polymer substrate by applying a compressive strain ε = 1.8%. Additional observations are:

– Both a circular buckle (line 1) and a half-circular buckle (line 3) with layer cracking are observed.

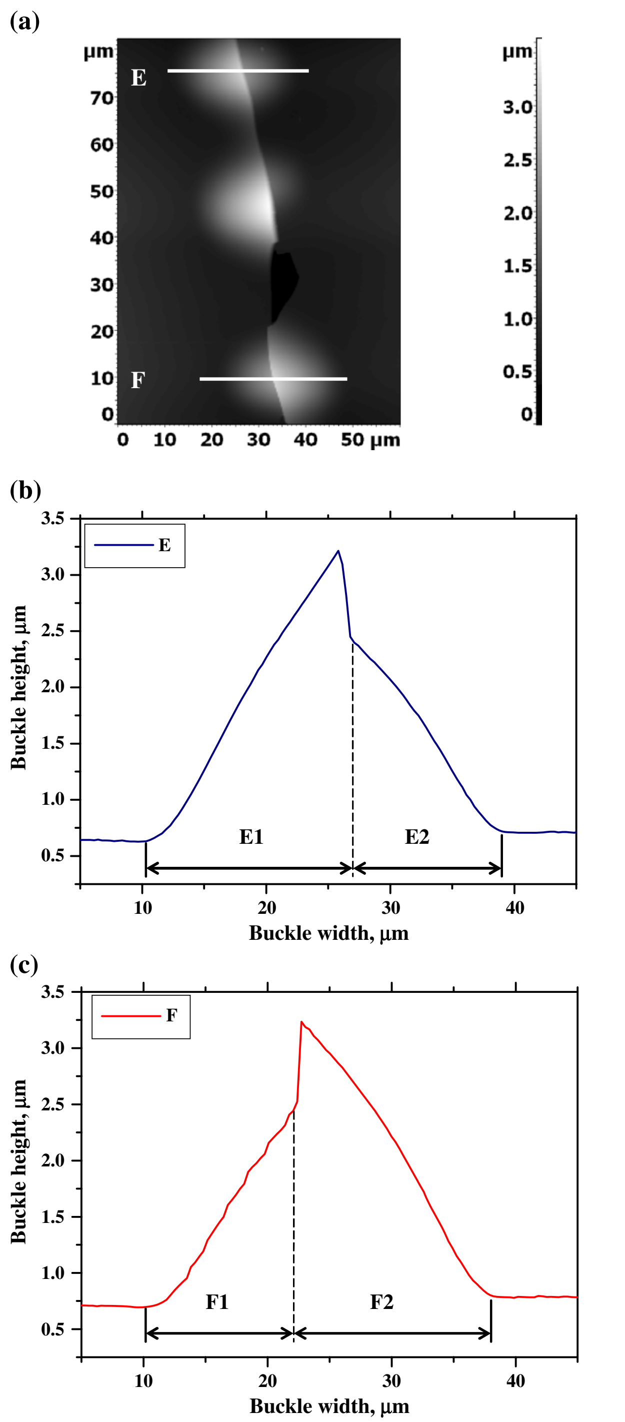

Fig. 10. (a) 2-D AFM image of asymmetric semi-circular buckle, (b) and (c) illustrations of the buckle profiles taken from the same direction indicated by line E and line F. The Si_3N_4 layer is 400 nm thick and deposited without oxygen plasma treatment. The applied uniaxial-compressive strain $\varepsilon = 1.52\%$.

– From the buckle profiles, the buckle width and height determined perpendicular to the axis of the circular buckle (line 1) are appeared roughly constant, $2b \cong 16.5$ μm and $w \cong 1.5$ μm,
– The layer between two buckles is also detached from the substrate, indicated by line 2, which apparently is a half-circular buckle.
– The width of the half-circular buckle (line 3) is approximately half the width of the circular buckle and the buckle height is approximately the same.

The effect of the oxygen plasma treatment and loading mechanism on the buckle morphology are obvious by comparing Figs. 3 and 10. Both have a 400 nm layer thickness. As illustrated in the former image, telephone-cord buckles are formed due to a combination of biaxial-compressive stresses in the thin layer with a poor adhesion at the interface, where oxygen plasma treatment didn't improve adhesion in this case. In the latter image, asymmetric semi-circular buckles are formed due to an additional uniaxial-compressive strain, where the layer is deposited without oxygen plasma treatment.

It is worth to note here that the buckle profiles of the asymmetric semi-circular buckles with layer cracking (Fig. 10b, c) are similar to those obtained for the telephone-cord buckle with layer cracking shown in Fig. 4c, d, in spite of the different buckle morphologies and loading mechanisms. Moreover, the buckle width for both is approximately the same $2b \cong 30$ μm while the buckle height for the telephone-cord with the layer cracking and circular buckle are $w = 3.6$ μm and $w = 2.6$ μm, respectively. Therefore, a transition from tele-

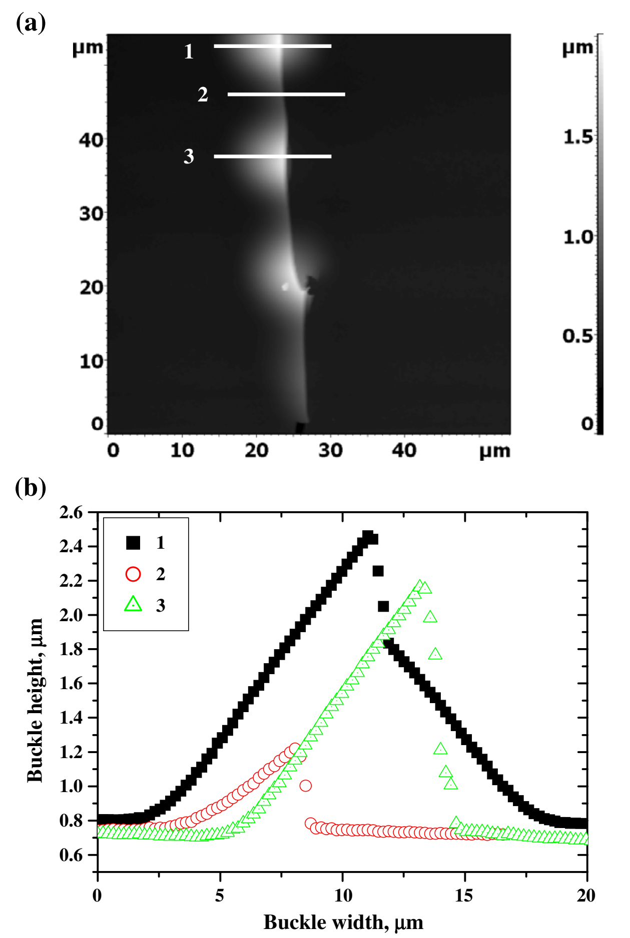

Fig. 11. (a) AFM image of buckling with layer cracking on top. (b) Buckle profile. The Si_3N_4 layer is 300 nm thick and deposited without oxygen plasma treatment. The applied uniaxial-compressive strain $\varepsilon = 1.8\%$.

phone-cord with layer cracking into circular or semi-circular buckle morphology may occur by adjusting the stress induced in the layered structures.

4. Conclusions

Experimental observations have been made to provide some understanding of the buckle morphology of compressed inorganic thin layers on a polymer substrate. The effect of surface treatment of the substrate prior to layer deposition is significant. Oxygen plasma treatment is found to enhance buckling of the Si_3N_4 layer from the polymer substrate. As a result, a straight and telephone-cord buckles were formed. On the other hand, no buckling was observed for layers prepared without oxygen plasma treatment. When the layers prepared without oxygen plasma treatment were under additional uniaxial-compressive strain, layer cracking is followed by a circular and a half-circular buckle formation perpendicular to the compression axis. The formation and propagation of a circular, half-circular and semi-circular buckle are well established. The buckle width and heights are found to increase with the applied compressive strain.

Investigations are in progress to link these experimental observations with numerical modeling taking into account the energy released from the substrate and the effect of the elastic mismatch on layer buckling and delamination.

Acknowledgements

The authors would like to thank the foundation for fundamental research on matter (FOM) and Philips for their financial support of this project. Kees Mutsaers for providing samples and Frank van Zon for his experimental support.

References

[1] J.W. Hutchinson, Z. Suo, Adv. Appl. Mech. 29 (1992) 63.
[2] J.W. Hutchinson, M.D. Thouless, E.G. Liniger, Acta Metall. 40 (1992) 295.
[3] M.D. Thouless, J. Am. Ceram. Soc. 76 (1993) 2936.
[4] M. Ortiz, G. Gioia, J. Mech. Phys. Solids 42 (1993) 531.
[5] M.W. Moon, H.M. Jensen, J.W. Hutchinson, K.H. Oh, A.G. Evans, J. Mech. Phys. Solids 50 (2002) 2355.
[6] D. Sarangi, S. Kumar, R. Bhattacharyya, Diamond Relat. Mater. 13 (2004) 1844.
[7] M.W. Moon, K.R. Lee, K.H. Oh, J.W. Hutchinson, Acta Mater. 52 (2004).
[8] B. Cotterell, Z. Chen, Int. J. Fract. 104 (2000) 169.
[9] H.H. Yu, J.W. Hutchinson, Int. J. Fract. 113 (2002) 39.
[10] M. George, C. Coupeau, J. Colin, J. Grilhé, Acta Mater. 53 (2005) 411.
[11] Y. Leterrier, L. Médico, P.C.P. Bouten and J. de Goede, Technical Note IST-2001-34215, FlexLED report D17.
[12] V.A. Soloukhin, J.C.M. Brokken-Zijp, G. de With, J. Mater. Res. 18 (2003) 507.
[13] K. Röll, J. Appl. Phys. 47 (1976) 3224.
[14] A.G. Evans, M.D. Drory, M.S. Hu, J. Mater. Res. 3 (1988) 1043.
[15] M.D. Thouless, J. Vac. Sci. Technol., A, Vac. Surf. Films 9 (1991) 2510.
[16] Z. Chen, B. Cotterell, W. Wang, Eng. Fract. Mech. 69 (2002) 597.
[17] J. Dundurs, J. App. Mech. 36 (1969) 650.
[18] P.C.P. Bouten, and M.A.J. van Gils, Technical Note PR-TN-2004/00580.
[19] M.W. Moon, J.W. Chung, K.R. Lee, K.H. Oh, R. Wang, A.G. Evans, Acta Mater. 50 (2002) 1219.
[20] J.W. Hutchinson, J. Mech. Phys. Solids 49 (2001) 1847.
[21] B. Audoly, Phy. Rev. Lett. 83 (1999) 4124.
[22] C.h. Bichler, T. Kerbstadt, H.-C. Langowski, U. Moosheimer, Surf. Coat. Technol. 112 (1999) 373.
[23] N. Matuda, S. Baba, A. Kinbara, Thin Solid Films 81 (1981) 301.
[24] W. Fang, J.A. Wickert, J. Micromechanics Microengineering 4 (1994) 116.